

Shock Waves in the Hydrodynamic Model for Semiconductor Devices

Carl L. Gardner*
Department of Computer Science
Duke University
Durham, NC 27706

Abstract

Numerical simulations of a family of steady-state electron shock waves (parametrized by the amount of heat conduction) in a one micron Si semiconductor device at 77 K are presented, using a steady-state upwind method. The electron shock wave has a finite width which scales linearly with the amount of heat conduction.

Comparisons of the hydrodynamic simulations with a Monte Carlo simulation of Laux using the DAMOCLES program are also presented. The hydrodynamic prediction of an electron shock wave [1] in Si at 77 K is confirmed by the DAMOCLES simulation of the Boltzmann equation. Good agreement between the two different methods for simulating the electron shock wave can be obtained by adjusting the amount of heat conduction in the hydrodynamic model.

1 Introduction

The hydrodynamic model treats the propagation of electrons in a semiconductor as the flow of a charged, heat conducting gas in an electric field. As such, the hydrodynamic model should perhaps be called *electrofluidynamics* (with heat conduction).

The electron gas has a soundspeed c [2] given by

$$c = \sqrt{T/m} \tag{1}$$

where T is the electron temperature in energy units and m is the effective electron mass. The electron flow may be either subsonic or supersonic. In the case of a

*Research supported in part by the National Science Foundation under grant DMS-8905872.

transition from supersonic flow to subsonic flow, an electron shock wave will in general develop in the hydrodynamic model.

The shock wave actually enhances electron flow in the channel of an $n^+ - n - n^+$ diode, allowing for higher electron densities, velocities, and currents [1]. The shock profile is no more dramatic than the effects of junctions in the diode.

In Si at $T_0 = 300$ K, $c = \sqrt{\alpha} 1.3 \times 10^7$ cm/s where $T = \alpha T_0$, while at $T_0 = 77$ K, $c = \sqrt{\alpha} 6.6 \times 10^6$ cm/s. The electron saturation velocity $v_s \approx 10^7$ cm/s at 300 K, and $v_s \approx 1.25 \times 10^7$ cm/s at 77 K. Thus it is difficult (though not impossible [1]) to produce an electron shock wave in Si at room temperature, but easy at liquid nitrogen temperature [1].

I will present numerical simulations of a family of steady-state electron shock waves (parametrized by the amount of heat conduction) in a one micron semiconductor device at 77 K, using a steady-state upwind method. The electron shock wave has a finite width which scales linearly with the amount of heat conduction. I will present numerical evidence that the shock width goes to zero as the amount of heat conduction in the model goes to zero.

I will also present comparisons of the hydrodynamic simulations with a Monte Carlo simulation of Laux using the DAMOCLES [3] program. The DAMOCLES simulation of the Boltzmann equation confirms the hydrodynamic prediction of an electron shock wave [1] in Si at 77 K. Good agreement between the two different methods for simulating the electron shock wave can be obtained by adjusting the amount of heat conduction in the hydrodynamic model.

2 The hydrodynamic model

The hydrodynamic equations are

$$\frac{\partial n}{\partial t} + \nabla \cdot (n\mathbf{v}) = \left(\frac{\partial n}{\partial t} \right)_c \quad (2)$$

$$\frac{\partial \mathbf{p}}{\partial t} + \mathbf{v} \nabla \cdot \mathbf{p} + \mathbf{p} \cdot \nabla \mathbf{v} = -en\mathbf{E} - \nabla(nT) + \left(\frac{\partial \mathbf{p}}{\partial t} \right)_c \quad (3)$$

$$\frac{\partial W}{\partial t} + \nabla \cdot (\mathbf{v}W) = -en\mathbf{v} \cdot \mathbf{E} - \nabla \cdot (\mathbf{v}nT) - \nabla \cdot \mathbf{q} + \left(\frac{\partial W}{\partial t} \right)_c \quad (4)$$

$$\nabla \cdot (\epsilon \nabla \phi) = -e(N_D - N_A - n), \quad \mathbf{E} = -\nabla \phi \quad (5)$$

where n is the electron density, \mathbf{v} is the velocity, $\mathbf{p} = mn\mathbf{v}$ is the momentum density, e (> 0) is the electronic charge, \mathbf{E} is the electric field, T is the temperature in energy units, $W = \frac{3}{2}nT + \frac{1}{2}mnv^2$ is the energy density, \mathbf{q} is the heat flow vector, the subscript c indicates collision terms, ϵ is the dielectric constant, ϕ is the electric potential, N_D is the density of donors, and N_A is the density of

acceptors. Eq. (2) expresses conservation of electron number, Eq. (3) expresses conservation of momentum, Eq. (4) expresses conservation of energy, and Eq. (5) is Poisson’s equation for the electric potential.

The transport equations (2)–(4) were derived by Bløtekjær [4] as the first three moments of the Boltzmann equation. The moment expansion is closed at three moments by assuming the Fourier law for heat conduction

$$\mathbf{q} = -\kappa\nabla T \tag{6}$$

where for semiconductors the thermal conductivity $\kappa = \kappa(n, T, T_0, N_D + N_A)$.

Eqs. (2)–(4) are in conservation form, and may be written in terms of the variables n , \mathbf{v} , T , and ϕ . These variables represent the simplest choice for upwind methods.

In the absence of heat conduction ($\kappa = 0$ in Eq. (4)), Eqs. (2)–(4) are the Euler equations [5] of gas dynamics with source terms due to the collision terms and the electric field. Eqs. (2)–(4) are hyperbolic (5 modes) in this case, and the soundspeed $c = \sqrt{\gamma T/m}$. The polytropic gas constant $\gamma = \frac{5}{3}$ for the “monatomic” electron gas. There are five nonlinear waves in the model: two shock waves (with characteristic speeds $u \pm c$, where u is the velocity normal to the wave) and three contact waves (with characteristic speed u). Two contact waves may be labeled by a jump in the tangential velocity \mathbf{v}_T across the wave, and one wave by a jump in the temperature T . With heat conduction (nonzero κ), Eqs. (2)–(4) are hyperbolic (4 modes) plus parabolic (1 mode). The contact wave corresponding to a discontinuity in T has disappeared due to the parabolic heat conduction term $\nabla \cdot (\kappa\nabla T)$ in Eq. (4), and the soundspeed $c = \sqrt{T/m}$. The limit $\kappa \rightarrow 0$ is a singular limit, with a discontinuous change in the soundspeed and the number of nonlinear waves [2].

3 The $n^+ - n - n^+$ diode problem

The $n^+ - n - n^+$ diode models electron flow in the channel of a MOSFET, and exhibits hot electron effects at scales on the order of a micron. The diode consists of an n^+ “source” region, an n “channel” region, and an n^+ “drain” region (see Fig. 1).

Since the effects of holes may be neglected for the $n^+ - n - n^+$ diode problem, in Eq. (2)

$$\left(\frac{\partial n}{\partial t}\right)_c = 0. \tag{7}$$

The collision terms in Eqs. (3) and (4) are approximated in terms of momentum and energy relaxation times. For the relaxation times and the thermal conductivity, I take the Baccarani-Wordeman models [6], with τ_w modified from the

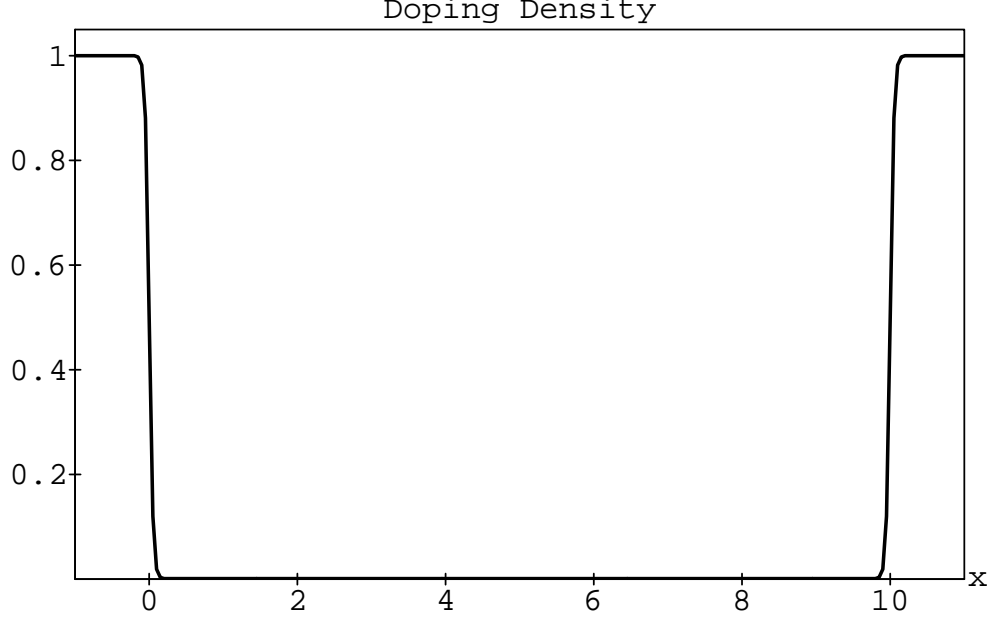


Figure 1: Doping profile in 10^{18} cm^{-3} for a 1 micron channel device at 77 K. x is in 0.1 microns for all figures.

summary in Ref. [7]:

$$\left(\frac{\partial \mathbf{p}}{\partial t}\right)_c = \frac{-\mathbf{p}}{\tau_p}, \quad \tau_p = m \frac{\mu_{n0} T_0}{e T} \quad (8)$$

$$\left(\frac{\partial W}{\partial t}\right)_c = \frac{-(W - \frac{3}{2}nT_0)}{\tau_w}, \quad \tau_w = \frac{m \mu_{n0} T_0}{2 e T} + \frac{3 \mu_{n0}}{2 e v_s^2} T_0 \quad (9)$$

where T_0 is the ambient device temperature, $\mu_{n0} = \mu_{n0}(T_0, N_D + N_A)$ is the low field electron mobility, and $v_s = v_s(T_0)$ is the saturation velocity. The models for τ_p and τ_w include the effects of electron-phonon and electron-impurity collisions. The thermal conductivity κ is specified by the Wiedemann-Franz law

$$\kappa = \kappa_0 \frac{\mu_{n0}}{e} n T_0 \quad (10)$$

where κ_0 is a positive constant.

In one dimension, the hydrodynamic model consists of three nonlinear conservation laws (for electron number, momentum, and energy), plus Poisson's equation for the electric potential:

$$f_n = \frac{d}{dx}(nv) = 0 \quad (11)$$

$$f_v = \frac{d}{dx}(m n v^2) - e n \frac{d\phi}{dx} + \frac{d}{dx}(nT) + \frac{m n v}{\tau_p} = 0 \quad (12)$$

$$f_T = \frac{d}{dx} \left(\frac{5}{2}nvT + \frac{1}{2}mnv^3 - env\phi \right) - \frac{d}{dx} \left(\kappa \frac{dT}{dx} \right) + \frac{\frac{1}{2}mnv^2 + \frac{3}{2}n(T - T_0)}{\tau_w} = 0 \quad (13)$$

$$f_\phi = \epsilon \frac{d^2\phi}{dx^2} + e(N - n) = 0. \quad (14)$$

For boundary conditions (assuming subsonic flow at the boundaries) I take charge neutral contacts ($n = N$) in thermal equilibrium ($T = T_0$) with the ambient temperature at x_{min} and x_{max} , with a bias V across the device: $e\phi(x_{min}) = T \ln(n/n_i)$ and $e\phi(x_{max}) = T \ln(n/n_i) + eV$, where n_i is the intrinsic electron concentration. If $\kappa_0 = 0$, then the energy equation (4) is hyperbolic rather than parabolic, and I drop one boundary condition and specify $n = N$ only at x_{min} .

The variables n , T , and ϕ are defined at the grid points $i = 0, 1, \dots, N - 1, N$, while the velocity v is defined at the midpoints of the elements l_i ($i = 1, \dots, N$) connecting grid points $i - 1$ and i . The boundary conditions specify n , T , and ϕ at $i = 0$ and $i = N$. Eqs. (11), (13), and (14) are enforced at the interior grid points $i = 1, \dots, N - 1$, while Eq. (12) is enforced at the midpoints of the elements l_i , $i = 1, \dots, N$. The discrete equations are then derived by using the second upwind method.

Eqs. (11)–(14) have the form

$$\begin{bmatrix} f_n \\ f_v \\ f_T \\ f_\phi \end{bmatrix} = \frac{d}{dx} \begin{bmatrix} vg_n \\ vg_v \\ vg_T \\ 0 \end{bmatrix} + \begin{bmatrix} 0 \\ h_v \\ h_T \\ h_\phi \end{bmatrix} + \begin{bmatrix} 0 \\ s_v \\ s_T \\ s_\phi \end{bmatrix} = 0 \quad (15)$$

where

$$g_n = n, \quad g_v = mnv, \quad g_T = \frac{5}{2}nT + \frac{1}{2}mnv^2 - env\phi \quad (16)$$

$$h_v = -en \frac{d\phi}{dx} + \frac{d}{dx}(nT), \quad h_T = -\frac{d}{dx} \left(\kappa \frac{dT}{dx} \right), \quad h_\phi = \epsilon \frac{d^2\phi}{dx^2} \quad (17)$$

and where the source terms s_v , s_T , and s_ϕ depend only on n , v , and T . In the second upwind method, the advection terms $d(vg)/dx$ in Eq. (15) are discretized using second upwind differences

$$\frac{d}{dx}(vg)_i \approx (v_{i+1}g_R - v_i g_L)/\Delta x \quad (18)$$

where

$$g_R = \begin{cases} g_i & (v_{i+1} > 0) \\ g_{i+1} & (v_{i+1} < 0) \end{cases}, \quad g_L = \begin{cases} g_{i-1} & (v_i > 0) \\ g_i & (v_i < 0) \end{cases} \quad (19)$$

and central differences are used for h_v , h_T , and h_ϕ . Recall that the velocity v_{i+1} is located at the midpoint of element l_{i+1} .

To linearize the discretized version of Eqs. (11)–(14), I use Newton’s method:

$$J \begin{bmatrix} \delta n \\ \delta v \\ \delta T \\ \delta \phi \end{bmatrix} = - \begin{bmatrix} f_n \\ f_v \\ f_T \\ f_\phi \end{bmatrix} = -f, \quad \begin{bmatrix} n \\ v \\ T \\ \phi \end{bmatrix} \leftarrow \begin{bmatrix} n \\ v \\ T \\ \phi \end{bmatrix} + t \begin{bmatrix} \delta n \\ \delta v \\ \delta T \\ \delta \phi \end{bmatrix} \quad (20)$$

where J is the Jacobian and t is a damping factor [8] between 0 and 1, chosen to insure that the norm of the residual f decreases monotonically. The Newton method converges quadratically.

Physical parameters. In silicon, the effective electron mass $m = 0.24 m_e$ at 77 K, where m_e is the electron mass, $\epsilon = 11.7$, and $n_i = 2.84 \times 10^{-20} \text{ cm}^{-3}$ at 77 K. I use the following model for μ_{n0} [6, 7] at 77 K:

$$\mu_{n0}(T0 = 77 \text{ K}, N_i) = \frac{\Delta\mu}{1 + (N_i/N_{ref})^\alpha} \quad (21)$$

$$\Delta\mu = 18000 \frac{\text{cm}^2}{\text{Vs}} \quad (22)$$

$$N_{ref} = 1.44 \times 10^{15} \text{ cm}^{-3} \quad (23)$$

$$\alpha = 0.659 \quad (24)$$

where $N_i = N_D + N_A$ is the total impurity concentration. The value for $\Delta\mu$ is taken from Monte Carlo simulations of pure Si at 77 K [9]. I take $v_s = 1.25 \times 10^7 \text{ cm/s}$.

4 Hydrodynamic computations of the electron shock waves

I will present simulations of the $n^+ - n - n^+$ diode in which a shock profile develops in the channel as the supersonic flow on entering the channel breaks to a subsonic flow, in analogy with gas dynamical flow in a Laval nozzle¹. The $n^+ - n - n^+$ doping of the diode corresponds to the converging/diverging geometry of the Laval nozzle.

The hydrodynamic shocks simulated below have a more complicated structure than shocks supported by the Euler equations of gas dynamics, due to the heat conduction term $\nabla \cdot (\kappa \nabla T)$ in Eq. (4), the relaxation time source terms in Eqs. (3) and (4), and the coupling of the electron gas to the electric field. A shock wave for the inviscid Euler equations is an exact discontinuity in n , v , and T , where v is the normal velocity of the gas [5]. In gas dynamics with heat conduction and

¹See Ref. [10] for an analysis of a steady-state shock wave in a Laval nozzle.

viscosity, a shock wave varies rapidly but smoothly over a short viscous length scale [5, 11, 12].

With heat conduction and no viscosity, the situation is more complex [11, 12]. In the frame of the shock, the flow ahead of the shock is supersonic and behind the shock is subsonic. If the Mach number M of the flow ahead of the shock is greater than one but less than a critical Mach number M_c , then the shock is a spread-out smooth profile. If $M > M_c$, then there is an outer profile to the shock wave with an inner exact discontinuity [11]. ($M_c = v_c/c \approx 1.74$ for a polytropic gas with $\gamma = 5/3$, where $c = \sqrt{T/m}$.)

Thus the traditional hyperbolic discontinuous shock wave of gas dynamics ($\kappa_0 = 0$) is spread out due to the parabolic heat conduction term. In other words, the electron shock waves in the hydrodynamic model have both parabolic and hyperbolic aspects.

I will present numerical evidence that the width of the outer shock profile scales linearly with κ_0 in Eq. (10). Thus in the limit of vanishing heat conduction ($\kappa_0 \rightarrow 0$), I obtain the traditional discontinuous shock wave of gas dynamics.

For the shock computations, I take a diode consisting of a 0.1 micron source, a 1.0 micron channel, and a 0.1 micron drain. In the n^+ region, the doping density $N = 10^{18} \text{ cm}^{-3}$ at 77 K, while in the n region $N = 10^{15} \text{ cm}^{-3}$ at 77 K (see Fig. 1). (I use a hyperbolic tangent fitting over ± 0.05 microns at the junctions.) The ambient device temperature $T_0 = 77 \text{ K} = 0.00665 \text{ eV}$.

Figs. 2–5 present a family of electron shock waves at $V = 1$ volt with 240 grid intervals². The shock profile is most clearly visible in the velocity plots (Fig. 2). For comparison’s sake, the DAMOCLES velocity is also plotted. The flow is supersonic at the velocity peaks just inside the channel, and subsonic at the end of the waves where the velocity makes a “bend” to the plateau in the channel. The width of the outer shock profile is roughly defined as the distance between where the wave “breaks” after the velocity peak and the beginning of the velocity plateau where v falls below the soundspeed c (see Figs. 3 and 4). To automate the calculation of the shock widths, I will define the shock width as

$$\text{width} \equiv (v_{max} - v_{min}) / \max\{|\Delta v / \Delta x|\} \quad (25)$$

over the wave, where Δv is the change in v over Δx . The Mach numbers and widths of the shock waves are presented in Table 1. The width of the shock wave shows an approximately linear scaling with κ_0 in the range $0 \leq \kappa_0 \leq 0.5$. For $0.1 > \kappa_0 \rightarrow 0$, the width of the computed shock wave is dominated by numerical and artificial viscosity effects. On the other hand, as κ_0 increases beyond 0.5, the width of the shock wave becomes harder and harder to define, due to the spreading out of the wave.

²The simulation of the 77 K shock wave has converged under mesh refinement with 240 grid intervals. See Ref. [1].

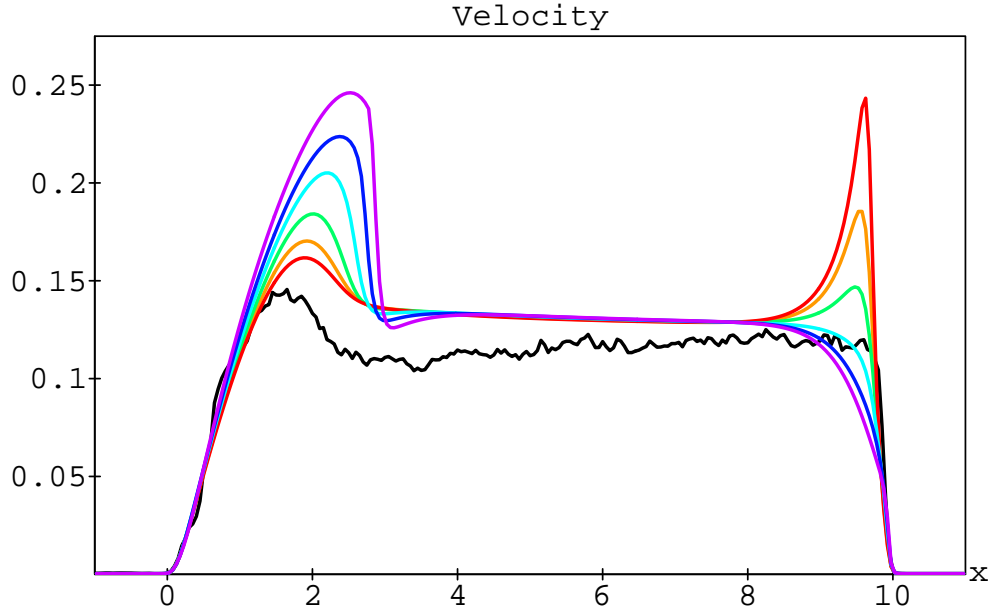


Figure 2: Electron velocities in 10^8 cm/s for $V = 1$ volt, 1 micron channel, 77 K, $\kappa_0 = 0$ (violet), 0.1 (dark blue), 0.25 (light blue), 0.5 (green), 0.75 (orange), and 1.0 (red). The black jagged curve is the DAMOCLES result.

κ_0	Mach number	width
0	3.8	0.16
0.1	3.2	0.20
0.25	2.8	0.31
0.5	2.4	0.45
0.75	2.2	0.51
1	2.0	0.55

Table 1: Mach numbers and widths (in 0.1 microns) of the electron shock waves vs. the amount of heat conduction κ_0 .

Note that there is an unphysical velocity “spike” near the channel–drain junction for $\kappa_0 \geq 0.25$. However all the “spikes” are subsonic.

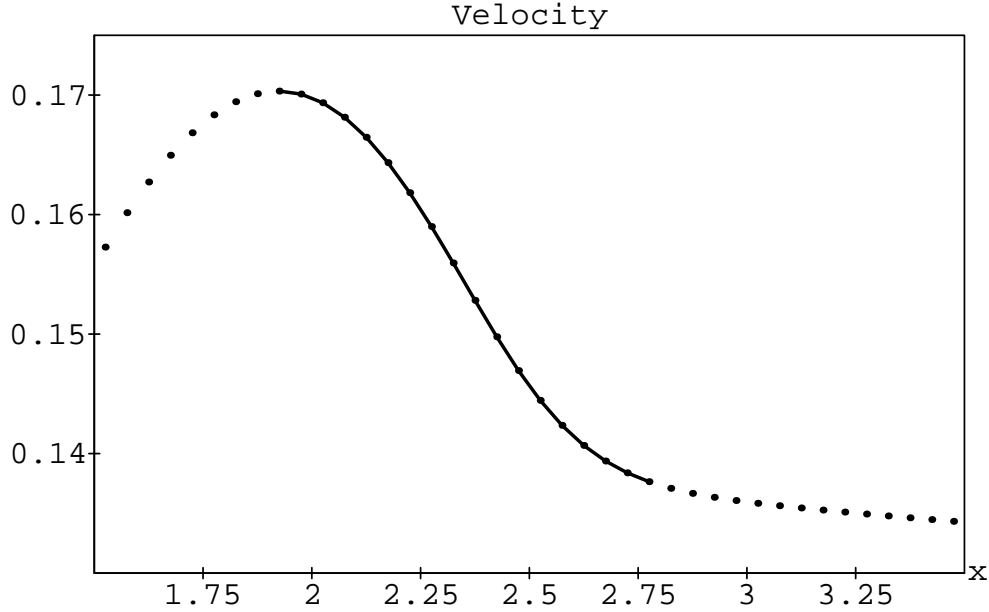


Figure 3: Detail of electron velocity in 10^8 cm/s for $\kappa_0 = 0.75$, $V = 1$ volt, 1 micron channel, 77 K, illustrating the “width” of the hyperbolic/parabolic shock wave (solid curve) spread out by the large amount of heat conduction in the hydrodynamic model.

Fig. 4 is a detail of the velocity plot for $\kappa_0 = 0$, showing the resolution of a discontinuous shock wave over $\sim 4\Delta x$. A small amount of explicit artificial viscosity of the form

$$\nu \max\{|v| + c\} \Delta x m \frac{d^2(nv)}{dx^2} \quad (26)$$

with $\nu = 0.03$ is necessary on the right hand side of Eq. (12) to eliminate oscillations ahead of the shock wave in this case. The shock wave can be resolved over $\sim 2\Delta x$ using a high-order ENO upwind scheme [13].

Fig. 5 demonstrates that the average electron energy is not very sensitive to the amount of heat conduction in the hydrodynamic model. Again the DAMOCLES average energy is shown for the sake of comparison. Note that the hydrodynamic energy with the Baccarani-Wordeman models is consistently too high.

Also note the evidence for an inner discontinuous shock in the average energy curves for $\kappa = 0.1$ and 0.25, since a discontinuity in dT/dx implies a discontinuous jump in v for the inner shock wave.³

³Integrating Eq. (13) over a wave yields $1/2mnv[v^2] = \kappa[dT/dx]$, where $[\psi]$ indicates the jump $\psi_+ - \psi_-$ across the wave [1].

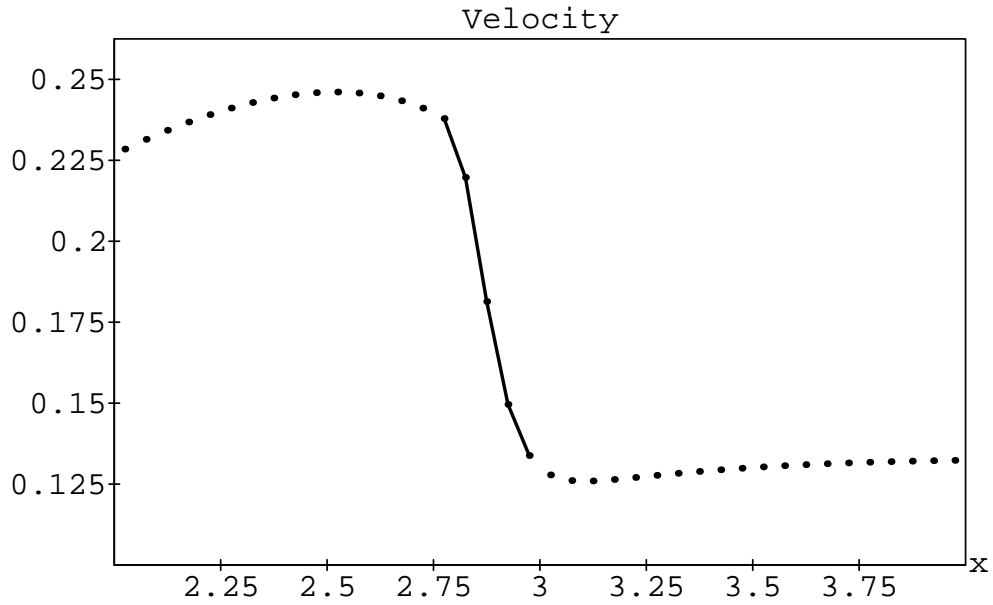


Figure 4: Detail of electron velocity in 10^8 cm/s for $\kappa_0 = 0$, $V = 1$ volt, 1 micron channel, 77 K, showing the traditional discontinuous shock wave of gas dynamics.

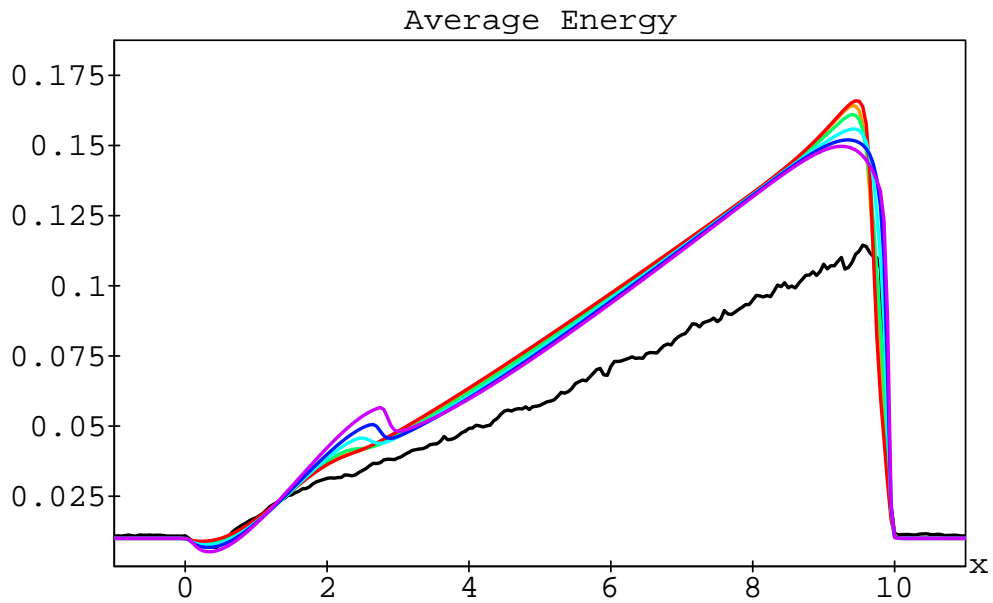


Figure 5: Average electron energy in eV for $V = 1$ volt, 1 micron channel, 77 K, $\kappa_0 = 0$ (violet), 0.1 (dark blue), 0.25 (light blue), 0.5 (green), 0.75 (orange), and 1.0 (red). The black jagged curve is the DAMOCLES result.

5 Comparison of hydrodynamic and Monte Carlo computations

The “best fit” hydrodynamic simulation uses a two-parameter fit on the amount of heat conduction, with $\kappa_{0L} = 0.75$ at the source–channel junction and $\kappa_{0R} = 0.3$ at the channel–drain junction. In the channel, κ_0 is linearly interpolated between κ_{0L} and κ_{0R} . Fig. 6 shows the DAMOCLES vs. “best fit” hydrodynamic electron velocity. The DAMOCLES velocity exhibits a Mach 2.2 shock profile (spread out due to heat conduction) based on both internal evidence⁴ and comparison with the hydrodynamic simulations.

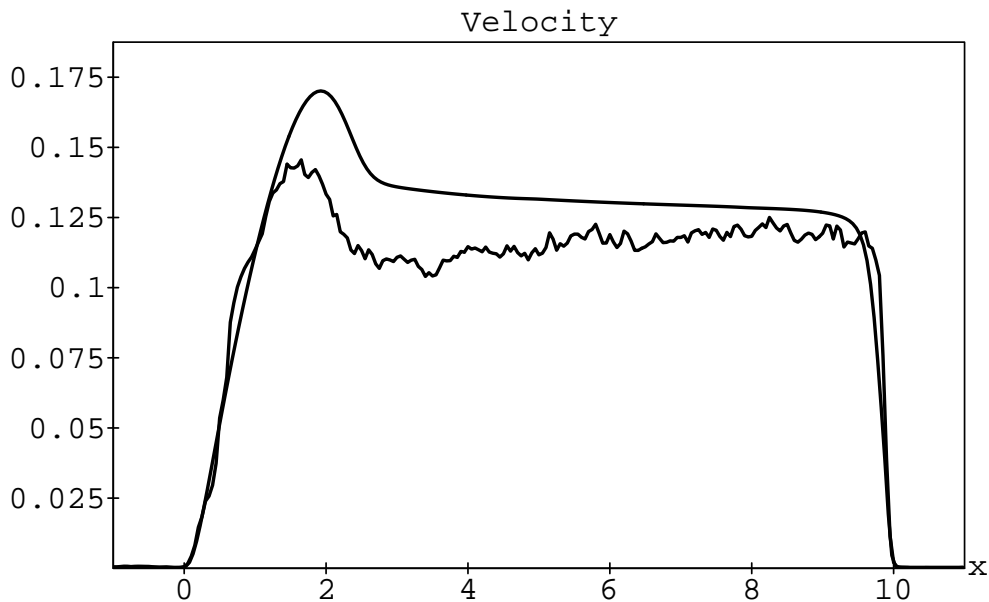


Figure 6: DAMOCLES vs. “best fit” hydrodynamic electron velocity in 10^8 cm/s for $V = 1$ volt, 1 micron channel, 77 K.

The average electron energies are plotted in Fig. 7. The DAMOCLES simulation indicates two electron temperatures near the channel–drain junction: “hot” 928 K electrons flowing from the channel, and “cold” 77 K electrons diffusing from the drain. This feature of the $n^+ - n - n^+$ diode was pointed out in Ref. [14]. The “best fit” hydrodynamic temperature with the Baccarani-Wordeman models again is too high as shown in Fig. 8. The peak electron temperature with the hydrodynamic model is approximately 1100 K.

⁴The electron temperature $T \approx 77$ K at the shock wave. Using the effective electron mass approximation, $M = v/c = v/\sqrt{T/m} \approx 2.2$.

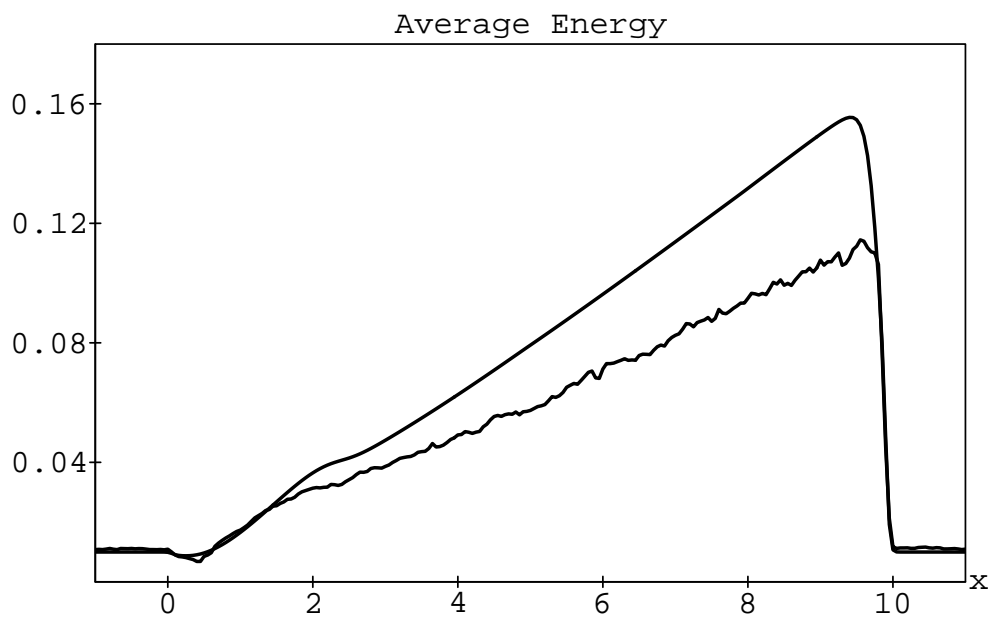


Figure 7: DAMOCLES vs. “best fit” hydrodynamic average electron energy in eV for $V = 1$ volt, 1 micron channel, 77 K.

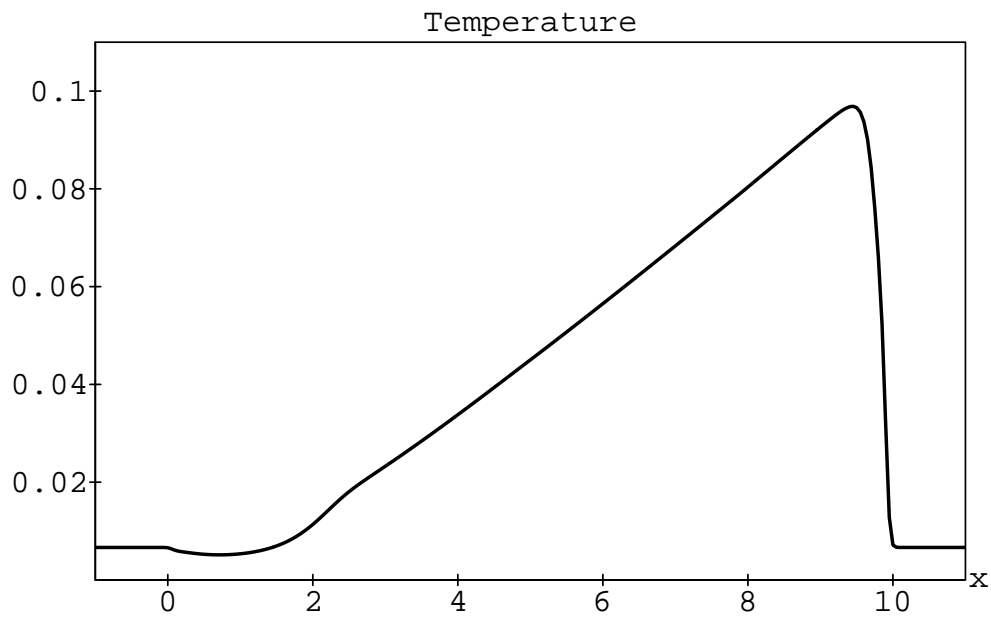


Figure 8: Electron temperature in eV for the “best fit” hydrodynamic simulation for $V = 1$ volt, 1 micron channel, 77 K.

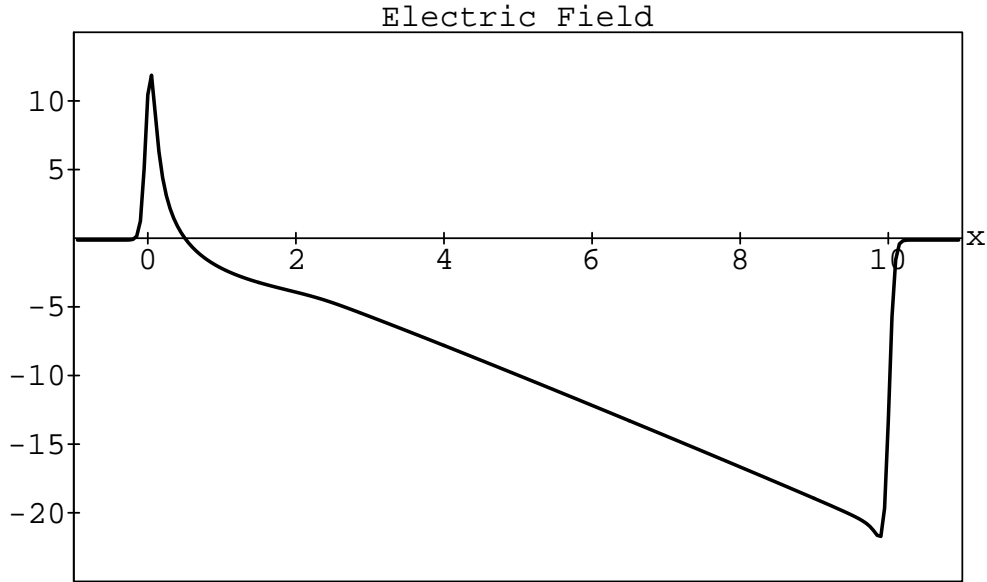


Figure 9: Electric field in kV/cm for the “best fit” hydrodynamic simulation for $V = 1$ volt, 1 micron channel, 77 K.

The electric field is shown in Fig. 9. The hydrodynamic and DAMOCLES electric potentials basically agree to within the plotting line width.

6 Conclusion

Good agreement between the hydrodynamic and Monte Carlo methods for simulating the electron shock wave can be obtained at a cost of adjusting the amount of heat conduction in the hydrodynamic model with two parameters κ_{0L} and κ_{0R} . This indicates that the Wiedemann-Franz law (10) or even the Fourier law (6) is incorrect, and a better model for heat conduction is essential for making quantitative predictions using the hydrodynamic model.

By using different models for τ_p and τ_w , I expect that better quantitative agreement between the DAMOCLES and hydrodynamic results can be obtained.

The velocity is the variable most sensitive to the amount of heat conduction in the hydrodynamic model. Thus if the average electron energy is physically the most important variable, then the exact value of κ_0 is not very important.

Both internal evidence and comparison with hydrodynamic simulations suggest that the “velocity overshoot” in the DAMOCLES velocity plot should be interpreted as a spread-out Mach 2.2 shock wave. Thus the hydrodynamic prediction of an electron shock wave [1] in Si at 77 K has been confirmed by Monte

Carlo simulation of the Boltzmann equation.

Acknowledgement

I would like to thank Steven Laux of the IBM Thomas J. Watson Research Center for providing the DAMOCLES results.

References

- [1] C. L. Gardner, “Numerical simulation of a steady-state electron shock wave in a submicrometer semiconductor device,” *IEEE Transactions on Electron Devices*, vol. 38, pp. 392–398, 1991.
- [2] C. L. Gardner, J. W. Jerome, and D. J. Rose, “Numerical methods for the hydrodynamic device model: Subsonic flow,” *IEEE Transactions on Computer-Aided Design of Integrated Circuits and Systems*, vol. 8, pp. 501–507, 1989.
- [3] M. V. Fischetti and S. E. Laux, “Monte Carlo analysis of electron transport in small semiconductor devices including band-structure and space-charge effects,” *Physical Review B*, vol. 38, pp. 9721–9745, 1988.
- [4] K. Bløtekjær, “Transport equations for electrons in two-valley semiconductors,” *IEEE Transactions on Electron Devices*, vol. ED-17, pp. 38–47, 1970.
- [5] R. Courant and K. O. Friedrichs, *Supersonic Flow and Shock Waves*. New York: Springer-Verlag, 1948.
- [6] G. Baccarani and M. R. Wordeman, “An investigation of steady-state velocity overshoot effects in Si and GaAs devices,” *Solid State Electronics*, vol. 28, pp. 407–416, 1985.
- [7] S. Selberherr, “MOS device modeling at 77 K,” *IEEE Transactions on Electron Devices*, vol. 36, pp. 1464–1474, 1989.
- [8] R. E. Bank and D. J. Rose, “Global approximate Newton methods,” *Numerische Mathematik*, vol. 37, pp. 279–295, 1981.
- [9] M. V. Fischetti, “Monte Carlo simulation of transport in technologically significant semiconductors of the diamond and zinc-blende structures—Part I: Homogeneous transport,” *IEEE Transactions on Electron Devices*, vol. 38, pp. 634–649, 1991.
- [10] J. Glimm, G. Marshall, and B. Plohr, “A generalized Riemann problem for quasi-one-dimensional gas flows,” *Advances in Applied Mathematics*, vol. 5, pp. 1–30, 1984.
- [11] Ya. B. Zel’dovich and Yu. P. Raizer, *Physics of Shock Waves and High-Temperature Hydrodynamic Phenomena*. New York: Academic Press, 1966.
- [12] R. Menikoff and B. J. Plohr, “The Riemann problem for fluid flow of real materials,” *Reviews of Modern Physics*, vol. 61, pp. 75–130, 1989.
- [13] C. L. Gardner and E. Fatemi, “Analysis of the electron shock wave in the hydrodynamic model for semiconductor devices,” in preparation.

- [14] M. R. Pinto, W. M. Coughran, C. S. Rafferty, R. K. Smith, and E. Sangiorgi, "Device simulation for silicon ULSI," in *Computational Electronics: Semiconductor Transport and Device Simulation*, Boston: Kluwer Academic Publishers, 1991.